

“Elastic” Property of Mesoporous Silica Shell: For Dynamic Surface Enhanced Raman Scattering Ability Monitoring of Growing Noble Metal Nanostructures via a Simplified Spatially Confined Growth Method

Min Lin,^{†,§} Yunqing Wang,^{*,§} Xiuyan Sun,[†] Wenhai Wang,[§] and Lingxin Chen^{*,§}

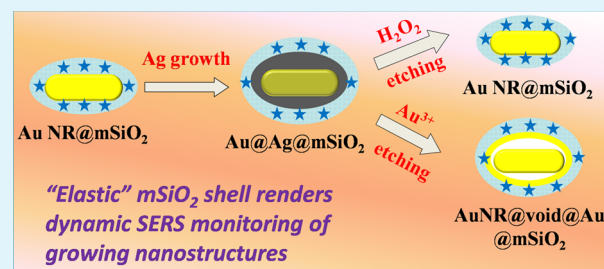
[†]School of Pharmacy, Yantai University, Yantai, Shandong 264005, China

[§]Key Laboratory of Coastal Environmental Processes and Ecological Remediation, Yantai Institute of Coastal Zone Research, Chinese Academy of Sciences, Yantai, Shandong 264003, China

Supporting Information

ABSTRACT: The Raman enhancing ability of noble metal nanoparticles (NPs) is an important factor for surface enhanced Raman scattering (SERS) substrate screening, which is generally evaluated by simply mixing as-prepared NPs with Raman reporters for Raman signal measurements. This method usually leads to incredible results because of the NP surface coverage nonuniformity and reporter-induced NP aggregation. Moreover, it cannot realize *in situ*, continuous SERS characterization. Herein, we proposed a dynamic SERS monitoring strategy for NPs with precisely tuned structures based on a simplified spatially confined NP growth method. Gold nanorod (AuNR) seed NPs were coated with a mesoporous silica (mSiO₂) shell. The permeability of mSiO₂ for both reactive species and Raman reporters rendered the silver overcoating reaction and SERS indication of NP growth. Additionally, the mSiO₂ coating ensured monodisperse NP growth in a Raman reporter-rich reaction system. Moreover, “elastic” features of mSiO₂ were observed for the first time, which is crucial for holding the growing NP without breakage. This feature makes the mSiO₂ coating adhere to metal NPs throughout the growing process, providing a stable Raman reporter distribution microenvironment near the NPs and ensuring that the substrate’s SERS ability comparison is accurate. Three types of NPs, i.e., core–shell Au@AgNR@mSiO₂, Au@AuNR@mSiO₂, and yolk–shell Au@void@AuNR@mSiO₂ NPs, were synthesized via core–shell overgrowth and galvanic replacement methods, showing the versatility of the approach. The living cell SERS labeling ability of Au@AgNR@mSiO₂-based tags was also demonstrated. This strategy addresses the problems of multiple batch NP preparation, aggregation, and surface adsorption differentiation, which is a breakthrough for the dynamic comparison of SERS ability of metal NPs with precisely tuned structures and optical properties.

KEYWORDS: surface enhanced Raman scattering, gold nanorod, mesoporous silica, core–shell nanoparticle, spatially confined growth



INTRODUCTION

Surface enhanced Raman scattering (SERS) tags with high sensitivity and multiplex labeling abilities have opened up a new avenue in the fields of bioimaging and biosensing.^{1–3} Since their discovery, the design and tailored synthesis of SERS tags with uniform, sensitive, and multiplexing properties have become permanent goals for researchers.^{4–6} Typically, a SERS tag is composed of a noble metal SERS nanosubstrate and surface-attached organic Raman reporter molecules with characteristic Raman signatures, in which metal nanosubstrates play a crucial role in the optical features of the tag. On one hand, noble metal nanoparticles (NPs) serve as scaffolds for SERS tags, which determine their morphology and physicochemical features. On the other hand, as Raman signal amplifiers, the size distribution, geometry, chemical composition, and localized plasmon resonance properties of NPs can influence the Raman electromagnetic enhancement ability and

the signal sensitivity of SERS tags. When this type of nanoprobe was first introduced, gold and silver nanospheres were widely used as substrates. Recently, more complicated and efficient SERS substrates have emerged, such as core–shell bimetallic NPs,^{7–10} alloy NPs,¹¹ hollow nanospheres,¹² and bilayered Raman-intense gold nanostructures with hidden tags (BRIGHTs)^{13–15} of interesting shapes and size monodispersity, which have enriched the diversity and greatly improved the optical performance of SERS tags.

With the various types of nanostructures available, one problem that has arisen is how to elaborately compare the Raman enhancing ability of structurally related NPs, such as core–shell NPs with different shell thicknesses or bimetallic

Received: December 3, 2014

Accepted: March 27, 2015

Published: March 27, 2015

nanoshells with different composition ratios. This problem has become a foundation for the tailored synthesis of single particle-based SERS tags. In general, the Raman enhancing ability of noble metal NPs is assessed by signal detection of the mixed solution of as-prepared NPs and Raman reporters of given concentration after the adsorption equilibrium. However, there were three problems with this method. First, the addition of reporters might induce an extreme nonuniformity of the surface coverage¹⁶ or the aggregation of NPs. It has been reported that each dimeric hotspot would be 700 times as strong as a monomer and each trimeric hotspot would be 2100 times as strong per unit area.¹⁷ Therefore, even very slight aggregation could greatly enhance the Raman signal intensity. Second, NPs of similar structures prepared by different methods usually have different surface coating ligands (citric acid, cetyltrimethylammonium bromide (CTAB), etc.). Thus, the interaction behavior and amount of the Raman reporters adsorbed on the NPs were different, which also caused distortion of the evaluation results. Third, a series of NPs with similar structures need to be presynthesized for comparison, which is laborious and cannot dynamically provide continuous SERS signal variation of growing NPs.

Recently, an “up-down” strategy was proposed for signal generation of SERS tags, in which a metal nanosubstrate was pre-coated with permeable polymers¹⁸ or mesoporous shells,^{19,20} followed by a Raman reporter mixing and infiltration step. The outer shells provided a uniform and “normalized” interface for Raman reporter adsorption for each type of encapsulated metal NP. Moreover, the shells prevented the random aggregation of NPs and ensured that the Raman enhancing ability could be evaluated from the desired nanostructures. Thus, this strategy successfully resolved the first two problems mentioned above; however, the third issue regarding dynamic SERS signal monitoring during the NP synthesis process remains a challenge.

The development of a spatially confined growth method for the fabrication of complicated noble metal nanostructures provided us with an opportunity. Using this method, seed NPs were pre-encapsulated in mesoporous silica (mSiO₂), followed by further NP core overcoating or etching reactions. The outer mSiO₂ shells have inherent advantages in that they allow the reactive molecules to enter the shell for NP growth and simultaneously protect the NPs from aggregation in complicated growth media.^{21–26} Thus far, this strategy has been applied in the fabrication of novel metal nanostructures as catalysts or theranostic nanoplatfoms. For example, core–shell Au–Pd bimetallic nanocrystals confined in silica nanorattles were prepared with enhanced catalytic activity, selectivity, and stability.²⁵ Au nanocrystals encapsulated in hollow mSiO₂ microspheres could be further coated with Pd or Pt shells using a “ship-in-a-bottle” growth method.²³ Spatially confined synthesis of core–shell gold nanocages@mSiO₂ by etching silver NP seeds has been reported for near-infrared controlled photothermal drug release.²⁴

Herein, we propose a systematic approach for dynamic SERS monitoring of metal NPs of changing morphology, inspired by a simplified spatially confined growth method using mSiO₂-coated gold nanorod (AuNR) as a model seed. The permeability of mSiO₂ for both reactive species and Raman reporters not only induces the reaction but also simultaneously indicates the Raman enhancing ability of instant NP products. Additionally, the mSiO₂ coating ensures the monodispersion of NPs in a Raman reporter-rich reaction system. Furthermore, we

observed the “elastic” feature of the mSiO₂ coating for the first time, which allowed for holding of the metal core during silver overcoating without breakage. Thus, the essential but laborious interior void generation in a typical spatially confined growth method²⁷ can be avoided, which simplifies the synthesis procedure. Three types of NPs, i.e., core–shell Au@AgNR@mSiO₂, Au@AuNR@mSiO₂, and yolk–shell Au@void@AuNR@mSiO₂ NPs, were synthesized via silver overgrowth and galvanic replacement methods, indicating the versatility of this approach. Moreover, the living cell SERS labeling ability of Au@AgNR@mSiO₂-based SERS tags was demonstrated.

EXPERIMENTAL SECTION

Materials. Chloroauric acid (HAuCl₄·3H₂O), silver nitrate (AgNO₃), sodium borohydride (NaBH₄), sodium hydroxide (NaOH), L-ascorbic acid (AA), crystal violet (CV), tetraethoxyorthosilicate (TEOS), and hydrogen peroxide (H₂O₂, 30%) were purchased from Sinopharm Chemical Reagent Co., Ltd. Hydroquinone, citric acid, and sodium citrate were obtained from Aladdin Reagent Co., Ltd. Cetyltrimethylammonium bromide (CTAB) was obtained from Sigma–Aldrich. MTT (3-(4,5-dimethylthiazol-2-yl)-2,5-diphenyltetrazolium bromide) was purchased from Invitrogen. RPMI-1640 medium, fetal bovine serum, penicillin–streptomycin solution, and trypsin–EDTA solution were purchased from Thermo Scientific. Deionized water was used in all of the experiments.

Characterization. The TEM images were acquired on a JEM-1400 transmission electron microscope (JEOL, Japan). SEM images and energy-dispersive X-ray spectra of the samples were obtained by using a field-emission microscope (Hitachi S-4800, Japan) equipped with an EX-350 energy dispersive X-ray microanalyzer (HORIBA EMAX Energy). UV/vis/NIR absorption spectra were recorded on a Thermo Scientific NanoDrop 2000/2000C spectrophotometer. SERS spectra were recorded by using a DXR Raman Microscope (Thermo Fisher, USA). A 632.8 nm He:Ne laser was focused by a 10× and 50× microscope objective for sample solution and cell measurement, respectively, with a power of 2 mW.

Preparation of AuNRs. AuNRs were synthesized using the seed-mediated growth method.²⁸ Briefly, the seed solution was prepared by reducing HAuCl₄ (0.5 mM, 2 mL) in CTAB (0.2 M, 2 mL) with freshly prepared ice-cold NaBH₄ (10 mM, 0.24 mL). After 2 h, 3.6 mL of resultant seed solution was added to a growth solution of HAuCl₄ (23 mM, 13 mL), CTAB (0.2 M, 200 mL), AgNO₃ (4 mM, 11.2 mL), and AA (0.08 M, 5 mL). The mixture was left overnight at 27–30 °C.

Preparation of AuNR@mSiO₂ NPs. AuNR@mSiO₂ NPs were synthesized according to a published procedure with minor modifications.²⁹ The as-prepared AuNRs (40 mL) were centrifuged (9500 r, 25 min) and dispersed in water (20 mL), followed by addition of NaOH (0.1 M, 200 μL) under stirring. Then, 20% TEOS in ethanol (200 μL) was added three times at intervals of 30 min under mixing. The resulting solution was allowed to further react for 48 h at 26–28 °C. The obtained AuNR@mSiO₂ core–shell NPs were then collected and washed 5 times with methanol (9000 r, 15 min) and then dispersed in 20 mL of water.

Preparation of Au@AgNR@mSiO₂ NPs. Purified AuNR@mSiO₂ NP solution (100 μL) was diluted to 500 μL, followed by addition of sodium citrate (38.8 mM, 20 μL), hydroquinone (0.1 M, 20 μL), and 438 μL of water. Then, citric acid (0.1 M, 50 μL) was added to the mixture to adjust the pH to approximately 4. Finally, a different volume of AgNO₃ solution (5 mM) was added to allow the reaction to proceed at 60 °C. To verify the elastic property of the mSiO₂ shell, H₂O₂ was used for selective dissolution of the Ag coating. Au@AgNR@mSiO₂ NPs prepared with 150 μL of AgNO₃ were dispersed in 1 mL of water, followed by the addition of different volumes (20, 50, and 100 μL) of H₂O₂ solution (30%, v/v). The reaction was allowed to proceed at room temperature, and the reaction rate was evaluated by monitoring the absorption spectra evolution of the solutions.

Preparation of Au@AuNR@mSiO₂ NPs. Purified AuNR@mSiO₂ NP solution (200 μ L) was diluted to 1 mL with water, followed by addition of HAuCl₄ solution (10 mM, 120 μ L). Then, AA (5 mM, 960 μ L) was injected into the mixture at a rate of 12 μ L min⁻¹.

Preparation of Au@void@AuNR@mSiO₂ NPs. To 1 mL of purified Au@AgNR@mSiO₂ NP (synthesized with 150 μ L of AgNO₃ solution), different volumes of HAuCl₄ solutions (0.1 mM) were injected at a rate of 5 μ L min⁻¹.

Preparation of Au@AgNRs. The as-prepared AuNRs (3 mL) were washed twice by centrifugation (9500 r, 25 min) and dispersed in water (3 mL). Then, CTAB solution (0.2 M, 10 mL) and 47 mL of water were added to the AuNR colloid to adjust the CTAB concentration to 0.033 M, followed by addition of AA (0.1 M, 220 μ L) and different volumes (0.2, 0.4, 0.6, 0.8, 1.0, and 1.2 mL) of AgNO₃ (0.01 M) under stirring. Finally, NaOH (0.1 M, approximately 3 mL) solution was added to initiate the deposition of the Ag shell by adjusting the pH of the mixture to approximately 10. The resulting solution was allowed to further react for 2 h at 27–30 °C.

Preparation of AuNRs@mSiO₂ and Au@AgNRs@mSiO₂ with Different mSiO₂ Thicknesses. The mSiO₂-coated NPs with different thicknesses were synthesized by adding different amounts of TEOS to the coating reaction mixtures, according to a published procedure with minor modifications.²⁹ For AuNRs@mSiO₂, the as-prepared AuNRs (40 mL) were centrifuged (9500 r, 25 min) and dispersed in water, followed by addition of NaOH (0.1 M, 200 μ L) under stirring. Then, different volumes of 20% TEOS in ethanol (90 and 180 μ L) were added three times at intervals of 30 min under mixing. The resulting solution was allowed to further react for 48 h at 26–28 °C. For Au@AgNR@mSiO₂, the Au@AgNR NPs (30 mL) were washed by centrifugation (7500 r, 15 min) and dispersed in CTAB solution (0.2 M, 7.5 mL), followed by a second round of centrifugation (7500 r, 15 min) and, finally, dispersion in water (7.5 mL). NaOH (0.1 M, 100 μ L) was added to the NP solution under stirring. Then, different volumes of 20% TEOS in ethanol (90 and 150 μ L) were added three times at intervals of 30 min under mixing. The resulting solution was allowed to further react for 48 h at 26–28 °C. The obtained NPs were then collected and washed 5 times with methanol (7000 r, 15 min) and then dispersed in water.

Cell Imaging. A breast-cancer-cell line (MCF-7) was grown as a monolayer in a humidified incubator at 37 °C in air/CO₂ (95:5) in an RPMI-1640 medium that was supplemented with 10% fetal bovine serum. For all experiments, the cells were harvested using trypsin and were resuspended in fresh medium before plating. MCF-7 cells (2.0 \times 10⁴) were seeded onto glass coverslips in a 24-well plate with 540 μ L of culture medium to allow the cells to attach. Then, 60 μ L of Au@AgNR@mSiO₂ NPs was added to the cells. After incubation for 4 h, the cell monolayer on the coverslips was repeatedly washed with PBS to remove the remaining particles and then sealed with a glass microscope slide. Observations were performed by Raman microscopy.

RESULTS AND DISCUSSION

Spatially Confined Growth of a Silver Shell on AuNR@mSiO₂. As shown in Figure 1a, AuNR@mSiO₂ was first fabricated and then subjected to silver overcoating via a spatially confined growth method. We selected Au@AgNR as a model product NP because of its ideal shape and size monodispersity. Additionally, the series of color changes during the NP growth could act as indicators, facilitating the judgment of the occurrence of the reaction and the thickness of the Ag layer. Moreover, Au@AgNR showed much greater SERS enhancing ability than the AuNR seed,³⁰ which would ensure a sharp contrast during dynamic SERS signal monitoring. The TEM images in Figure 1b,c illustrate that the AuNR seeds have an average aspect ratio of 3.6 and are encapsulated in mSiO₂ with a thickness of approximately 10 nm. The shape of the Au@AgNR@mSiO₂ NPs evolved with increasing Ag⁺ ion concentration in the growth solution under optimum reaction conditions. At lower volumes of AgNO₃ (25 μ L), the Ag

(a) Elastic property of mSiO₂ shell

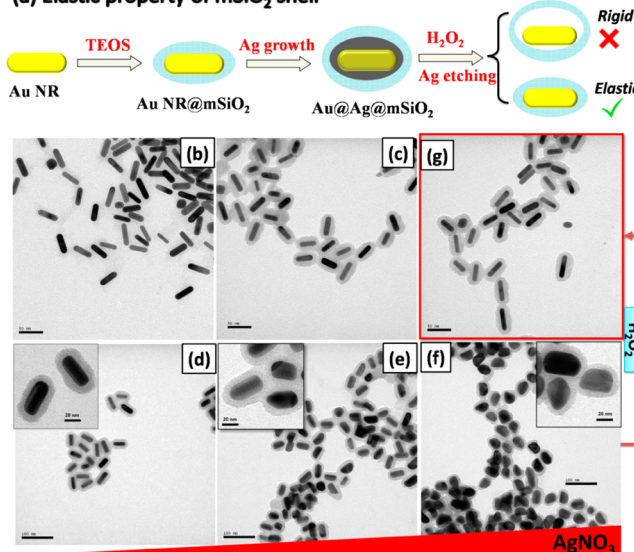
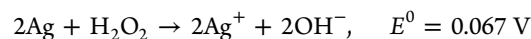


Figure 1. (a) Systematic illustration of the procedures for the fabrication of Au@AgNR@mSiO₂ NPs via the spatially confined growth method. AuNR@mSiO₂ NPs are first produced, followed by the Ag nanoshell overcoating onto the AuNR seed, which results in the expansion of the mSiO₂ coating. Further, introducing H₂O₂ leads to shrinkage of the mSiO₂ coating, indicating its elastic property. TEM images showing the morphologies of AuNR (b) and AuNR@mSiO₂ (c) as well as the evolution of Au@AgNR@mSiO₂ NPs obtained by adding 25 μ L (d), 75 μ L (e), and 150 μ L (f) of 5 mM AgNO₃ solutions. (g) TEM image of AuNR@mSiO₂ obtained by silver etching of the Au@AgNR@mSiO₂ shown in (f).

shell seemed to be homogeneous over the entire AuNR and the resulting bimetallic NP remained in the original cylindrical rod shape of the AuNR (Figure 1d). When the volume of AgNO₃ was increased to 75 μ L, an anisotropic Ag coating occurred, which resulted in Au@AgNRs with an orange slice-like shape (Figure 1e). When the volume was increased to 150 μ L, the width of the orange slice also increased (Figure 1f). This anisotropic growth method is consistent with Au@AgNR growth in free solution,³¹ indicating that the mSiO₂ shell did not influence the NP growth behavior. Additionally, it was observed that mSiO₂ compactly capped the growing bimetallic NPs but became thinner as a result of the swelling force from enlarged NPs (Figure S1, Supporting Information). This result revealed that the mSiO₂ shell was not rigid but rather elastic to some extent; thus, it permitted the growth of seed AuNRs while still supporting the greatly enlarged Au@AgNRs with tension. To further verify this finding, we dissolved the Ag shell of Au@AgNR by addition of H₂O₂. Under neutral conditions, the standard reduction potential of H₂O₂ ($E^0 = 0.867$ V) is higher than that of Ag⁺/Ag ($E^0 = 0.799$ V) and lower than that of Au³⁺/Au ($E^0 = 1.51$ V).²⁷ H₂O₂ could selectively remove the Ag shell based on the following reaction:



If the mSiO₂ shell was rigid, a cavity would appear between the AuNR and the mSiO₂ shell, forming a yolk–shell structure.²⁷ Interestingly, as shown in Figure 1g, the pre-expanded mSiO₂ shell contracted and adhered once again to AuNR, making the morphology of the recovered NP nearly identical to that of AuNR@mSiO₂, as shown in Figure 1c.

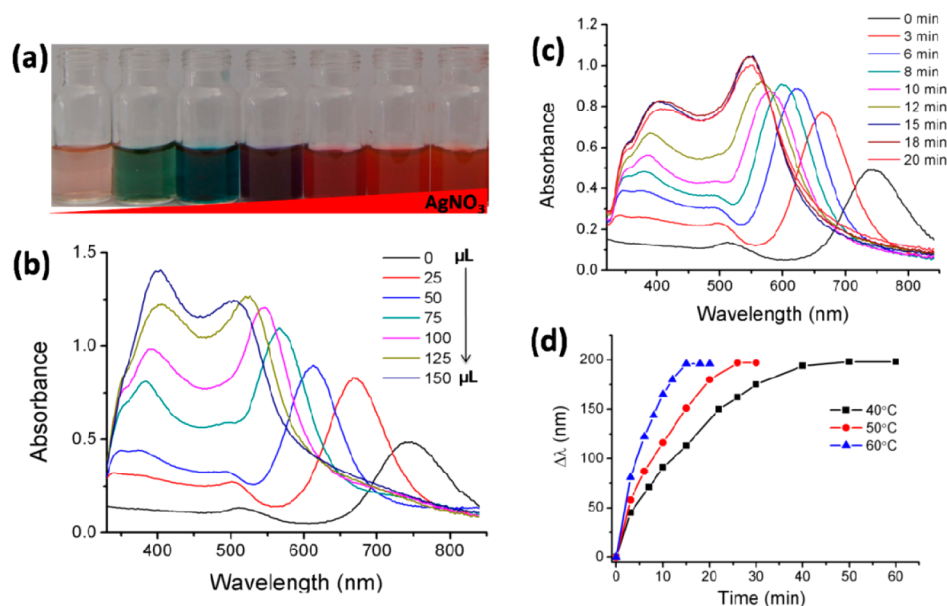


Figure 2. (a) Photographs of aqueous dispersions of AuNR@mSiO₂ before and after reaction with different volumes of a 5 mM AgNO₃ solution (0, 25, 50, 75, 100, 125, and 150 μL from left to right). (b) The corresponding UV-vis-NIR absorption spectra. (c) UV-vis-NIR absorption spectra from different reaction times. The amount of added AgNO₃ solution was 100 μL, and the reaction temperature was 60 °C. (d) Plots of the blue shifts of the longitudinal SPR band versus time for the samples prepared at 40, 50, and 60 °C. The amount of added AgNO₃ solution (5 mM) was 100 μL.

The elemental composition variation of the NP products was characterized by energy-dispersive X-ray spectra. As shown in Figure S2, Supporting Information, the silver content (atom percentage) of AuNRs@mSiO₂ NPs was 0.53%, which originates from the AuNR core. During the AuNR synthesis process, the addition of a trace volume of AgNO₃ was essential to regulate the rod shape.²⁸ For Au@AgNR@mSiO₂ NPs, after silver coating with 150 μL of AgNO₃, the Ag content increased to 11.09%. After silver etching by H₂O₂, the Ag content decreased to 1.34%, which was close to the background value of AuNR. These results confirm the overgrowth and dissolution of the Ag shell.

Dynamic Monitoring of Optical Properties. The reaction progress could also be indicated by a series of color changes of the NP solutions. As shown in Figure 2a, distinctive color changes were observed from pink of the AuNR seeds to green, blue, and finally orange of Au@AgNRs with increasing silver shell thickness. The corresponding UV-vis-NIR absorption spectra are presented in Figure 2b. The AuNR@mSiO₂ showed a longitudinal surface plasmon resonance (SPR) peak at 740 nm and a transverse SPR band centered at 511 nm. By increasing the amount of deposited Ag, the longitudinal SPR band obviously blue-shifted as a result of the decrease of the aspect ratio of AuNR during the Ag coating.³¹ In addition to the transverse SPR of AuNR, a new peak at approximately 340 nm appeared in the shorter wavelength region, which can be assigned to a transverse dipole resonance of the Ag shell. Moreover, the peak at 380 nm resulting from the transverse dipole resonance of electrons at the thick side of the Ag shell became stronger during silver growth. After adding H₂O₂ for silver etching, the longitudinal SPR peak of Au@AgNR@mSiO₂ gradually red-shifted to the absorption position of the AuNR seed, revealing a reverse process compared to the Ag shell growth profile in Figure 2. It was found that increasing the amount of H₂O₂ could accelerate the reaction, whereas the final SPR position of the products remained the same as that of the

AuNR seed, taking advantage of the etching selectivity of H₂O₂ (Figure S3, Supporting Information).

In most reported methods for spatially confined NP growth, the formation of yolk-shell structures is essential, in which the seed NPs are freely dispersed in the void of the mSiO₂ shell. Under this condition, the reactants pass through mSiO₂ and uniformly fill the cavity, serving as a confined microenvironment for reactions, which does not differ much from the condition in free solution. Comparatively, in our void-free strategy, the overcoating reaction occurs at the interface of the AuNR and the adhered mSiO₂, where the mass transfer speed of the reactants must be slower, leading to a reaction that is much more difficult to achieve.³² Temperature was a major factor affecting the mass transfer and the reaction speed;³³ thus, four temperatures were investigated. A control experiment indicated that the Ag overcoating cannot be accomplished at room temperature of 20 °C. As shown in Figure S4 (Supporting Information), the color of the solutions containing different amounts of AgNO₃ were all pale green after a 15 h reaction, and the SEM image showed the formation of nonuniform free silver NPs rather than Au@AgNR@mSiO₂. When the temperature was increased to above 40 °C, the core-shell NPs formed as indicated by the successive color change of the solution and the regular blue-shift of the longitudinal SPR peak (Figure 2c). Moreover, the reaction rate increased dramatically with the increase in temperature. By monitoring the blue-shift of the longitudinal SPR peak, it was determined that the terminal reaction time was approximately 40 min at 40 °C, whereas it decreased to 15 min at 60 °C. Moreover, the AuNR@mSiO₂NP washing procedure was another factor influencing the growth kinetics of the inner metal core. In this work, the AuNR@mSiO₂ NPs were washed 5 times with ethanol. If the NPs were only washed twice with water, the reaction occurred but the reaction time was prolonged from 15 min to approximately 20 min at 60 °C. This result is likely because of the hindering effect of the remaining CTAB in the mesopores of mSiO₂ preventing penetration of the reagents.

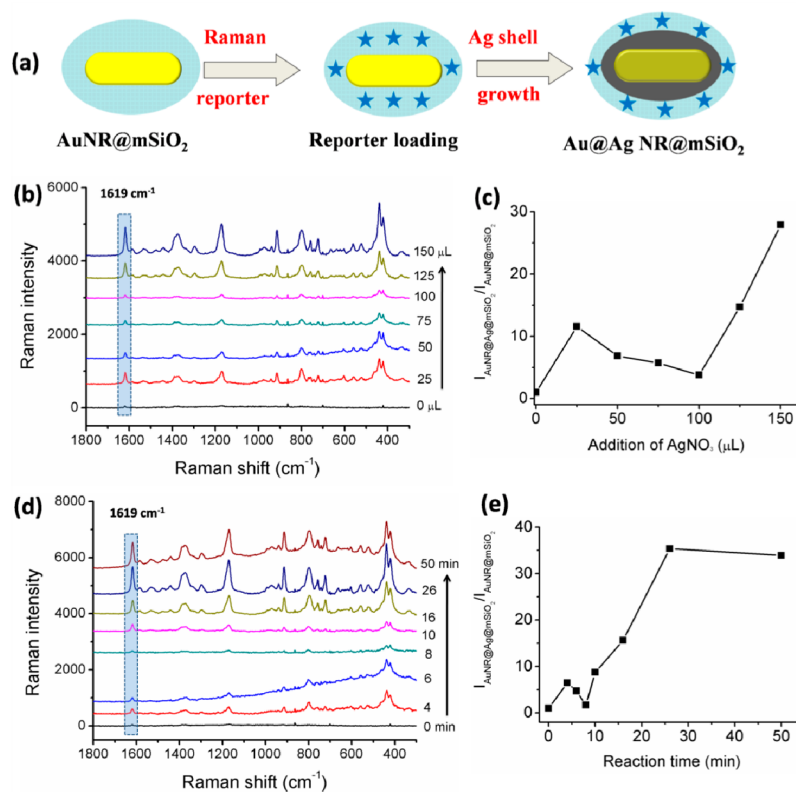


Figure 3. (a) Schematic of dynamic SERS monitoring of growing Au@AgNRs. The mSiO₂ coating allowed for the overcoating reaction, the Raman reporter adsorption and stabilization, and the monodispersity of NPs. (b) Raman spectra of Au@AgNRs@mSiO₂ NP solution prepared with different amounts of AgNO₃. (c) Raman signal intensity ratio of the CV peak at 1619 cm⁻¹ between Au@AgNRs@mSiO₂ and AuNRs@mSiO₂ NPs. (d) Raman spectra of AuNRs@mSiO₂ after different durations of exposure to 150 μL of AgNO₃ at 60 °C. (e) Plot showing the Raman intensity of the peak at 1619 cm⁻¹ from the growing NPs for different durations.

The reaction process was also influenced by the thickness of the mSiO₂ shell. For a AuNR@mSiO₂ NP sample with a mSiO₂ thickness of approximately 30 nm, the Ag overcoating could not occur even at 60 °C for 15 h because of slower reactant penetration as well as the increased mechanical strain strength of mSiO₂ (Figure S5, Supporting Information). To demonstrate the versatility of our void-free, spatially confined NP growth method based on the elastic property of mSiO₂, further Au coating on the AuNR seeds was also performed to achieve Au@AuNR@mSiO₂ with satisfactory results (Figure S6, Supporting Information).

Synthesizing these nanomaterials with good repeatability was a precondition for the dynamic study of the optical properties. Under the optimum synthesis conditions, the morphology of the grown NPs and the changing absorption spectral features could be reproduced. SEM characterization results showed that the morphologies of both AuNR@mSiO₂ and Au@AgNR@mSiO₂ (synthesized with 150 μL of AgNO₃) prepared in two batches were similar (Figure S7, Supporting Information).

The mSiO₂ synthesized using CTAB as a template possessed pore diameters of approximately 2 nm,^{34,35} which allowed for the molecular diffusion of Raman reporters and the ability to feel the electromagnetic field of the metal NPs. Additionally, the Raman reporters could be stabilized within the mSiO₂ shell in a three-dimensional manner, and the dispersed density remained unchanged during the growth process (Figure 3a). Therefore, the established *in situ* growth method could provide a facile method for evaluating SERS enhancing abilities of growing NPs of similar structure but with different metal

compositions. To test this idea, a given concentration of 10⁻⁶ M crystal violet (CV) was added to the Au@AgNRs growth medium and SERS spectra were collected with 632.8 nm excitation light. As shown in Figure 3b, the SERS intensity varied with increasing amounts of AgNO₃. When the volume of AgNO₃ was 25 μL, the SERS intensity increased compared to that of the AuNR@mSiO₂ seed solutions, mainly because of the shift of the longitudinal SPR to the laser excitation wavelength. For the samples in which 50 to 100 μL of AgNO₃ solution was added, a decreased intensity of the peaks was observed because the longitudinal SPR bands gradually shifted away from the wavelength of the 632.8 nm excitation.³⁶ Thereafter, the SERS intensity began to abruptly increase for samples with thicker Ag shells (Figure 3c). For the sample obtained by adding 150 μL of AgNO₃, the Raman intensity at 1619 cm⁻¹ was 28 times higher than that for AuNR@mSiO₂ (Figure S8, Supporting Information), which was attributed to the much greater Raman enhancing ability of Ag than Au.³⁷ The SERS signal variations could also be dynamically monitored during the Ag coating process. Figure 3d shows a typical set of SERS spectra collected at different time intervals in one reaction system containing 150 μL of AgNO₃. Overall, the SERS signal variation of the CV illustrated a similar “rise-fall-rise” principle. At 4 min, the intensity dramatically increased compared to that of the AuNR seed (Figure 3e). Within the range of 4 to 8 min, a decreasing intensity of peak 1619 cm⁻¹ was observed. An apparent fluorescence background could be observed, especially for the spectra collected at 6 min, suggesting that the fluorescence of the CV molecules was greatly enhanced by Au@AgNR at this

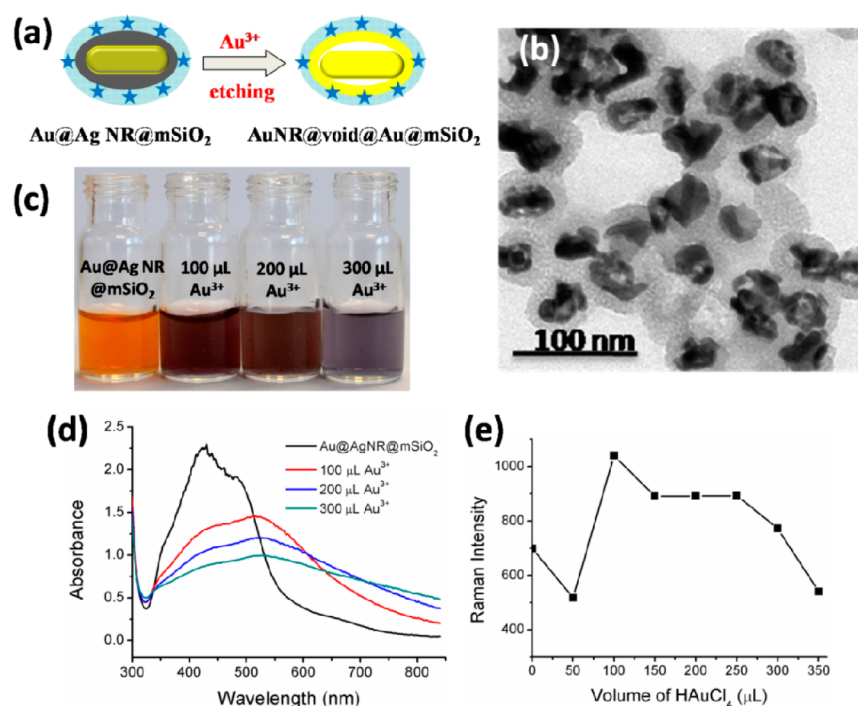


Figure 4. (a) Schematic illustration of the spatially confined galvanic replacement strategy for SERS-labeled AuNR@void@Au@mSiO₂ NPs. (b) TEM images of AuNR@void@Au@mSiO₂ NPs obtained by addition of 300 μL of 0.1 mM HAuCl₄ to 1 mL of Au@AgNR@mSiO₂ NPs. (c) Photographs of aqueous dispersions of AuNR@void@Au@mSiO₂ NPs before and after reaction with different volumes of 0.1 mM HAuCl₄ solution. (d) The corresponding UV–vis–NIR extinction spectra. (e) SERS intensity of CV-labeled samples with different volumes of HAuCl₄ solution.

growth stage. Then, the SERS signal continued to increase monotonically up to approximately 26 min, becoming nearly saturated with a further increase of the reaction time.

Rattle-structured Au@void@Au NPs have recently attracted much attention in the construction of theranostic platforms as a result of their enhanced photothermal efficiency and SERS enhancing ability compared to AuNR seeds.^{38–40} The *in situ* synthesis and SERS signal monitoring of this type of NPs were also demonstrated using our strategy by adding HAuCl₄ to the as-prepared Au@AgNR@mSiO₂ NPs (Figure 4a). TEM showed that yolk–shell metal structures formed after the replacement reaction. The mSiO₂ shell did not shrink and the overall size of the NPs did not change significantly (Figure 4b). The color of the NP solutions changed from orange to purple, corresponding to the structural changes, and the longitudinal SPR peak red-shifted toward the NIR region and experienced a large spectral broadening (Figure 4c,d). This broadening is likely attributed to the enhanced surface scattering of electrons in the nanocage walls.³⁸ Dynamic SERS monitoring revealed that, compared to Au@AgNR, the enhancing ability of this Au-rich rattle structure decreases gradually with the amount of HAuCl₄ but is still approximately 16 times greater than that of AuNR (Figure 4e).

To the best of our knowledge, this was the first reported strategy for elucidating the relationship between instant NP structures and Raman signal intensities in a real-time method. This strategy revealed several advantages: (1) facile handling and dynamic monitoring. The evolution of the silver shells also gave rise to a gradual change in the SERS properties for the colloidal systems, which could be easily monitored in one pot without the need for synthesizing a series of Au@AgNRs; (2) prevention of possible NP aggregation and the uniformity of Raman reporter adsorption on the metal substrate (interaction

speed and adsorbed amount). These two factors were difficult to precisely control in the system in which NPs and reporters were simply mixed. For comparison, we prepared a series of Au@AgNRs with different Ag contents for evaluation of the enhancing ability (Figure S9, Supporting Information). Because the synthesis medium was rich in CTAB, the obtained NPs needed to be washed with water. When CV was added to the NP solutions that were washed once, no Raman signal could be detected for all samples with various Ag shell thicknesses because the remaining CTAB coated on the NPs precluded the adsorption of CV onto the metal. However, if the NPs were washed twice, another problem arose. It was found that the SERS intensity of CV underwent an abrupt increase for the NPs with thicker Ag shells. This was attributed to the aggregation of NPs, observed by UV–vis–NIR absorption spectra, because the more sphere-like NPs had larger curvatures and more easily lost the protective CTAB coating during the second washing procedure. Our spatially confined, *in situ* growth method overcame these problems because the growth medium was CTAB-free and the Raman reporters were pre-concentrated and evenly distributed in mSiO₂ in a three-dimensional manner for generating SERS signals.⁴¹ Moreover, the protection of the elastic mSiO₂ shell prevented the aggregation of the grown NPs even after multiple washing steps.

It should be noted that the mSiO₂ shell became thinner as the inner core grew, which might be a factor influencing the Raman enhancing effect. The SERS intensity was highly dependent on the distance between the noble metal surface and the Raman reporters,^{42–44} which was theoretically and experimentally proved by two models. In Model 1, the noble metal substrate was covered by a pinhole-free, chemically uniform spacer shell (silica, Al₂O₃, carbon, etc.) with a

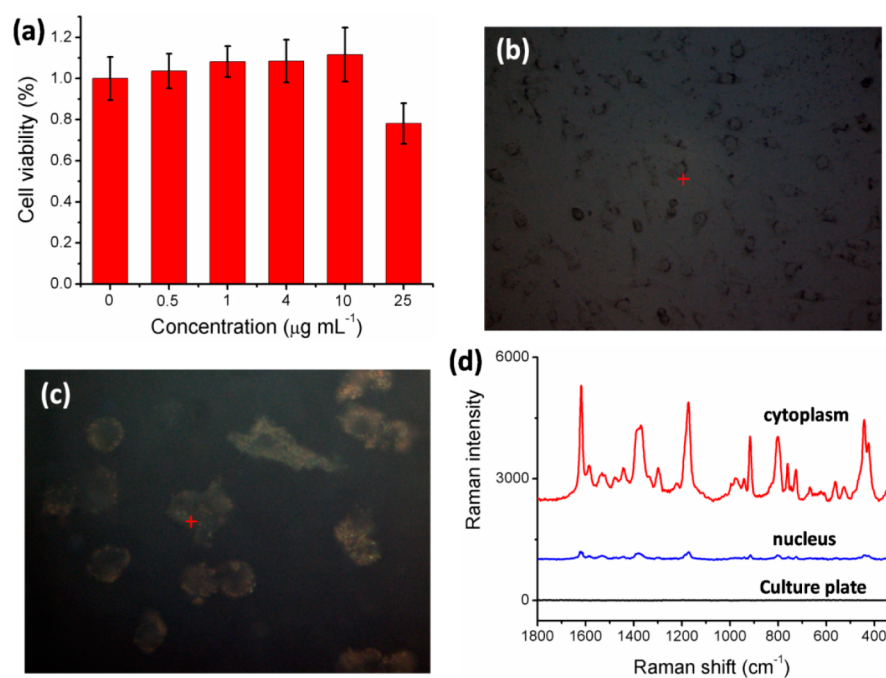


Figure 5. (a) Cytotoxicity assays of the CV-labeled Au@AgNRs@mSiO₂ NPs in MCF-7 cells. (b) Bright and (c) dark-field images of MCF-7 cells after incubating CV-labeled Au@AgNRs@mSiO₂ NPs for 4 h. The images were acquired with a 10× and a 50× objective lens, respectively. (d) Corresponding Raman spectra at different laser spots across one labeled MCF-7 cell.

controllable thickness of subnanometer up to several nanometers (Figure S10 a, Supporting Information). Then, Raman reporters were adsorbed on these materials with different coating thicknesses, and the SERS intensities were evaluated. It was found that the SERS intensity was strong only when the Raman reporters were very close to the metal surface (within approximately 2 nm). With increasing distance, the SERS intensity dropped dramatically, becoming nearly undetectable when the spacer thickness reached approximately 10 nm.^{42,43} One should experimentally observe the r^{-10} distance dependence:

$$I_{\text{SERS}} = [(a + r)/a]^{-10}$$

where I_{SERS} is the intensity of the Raman mode, a is the average size of the field-enhancing features on the surface, and r is the distance from the surface to the adsorbate.⁴² In Model 2, Raman reporter-modified linear molecules (DNA or polymer) were synthesized and then attached to the metal NP. Here, the linear molecule acted as a spacer (Figure S10b, Supporting Information). In this strategy, the distance between the reporter and the metal surface could be precisely defined and the reporter numbers on single metal NP could be stabilized. Then, the metal NP was subjected to further growth. With the silver growth, the spacer molecule is entrapped in the shell and the distance between the reporter and the NP surface is shortened. An apparent increase in the SERS intensity was thus observed during the NP growth process.⁴⁴

However, the model proposed in our experiment (Model 3) was different from the former two, in which the SERS intensity was not as sensitive to the variation of mSiO₂ thickness (Figure S10c, Supporting Information). In our case, Raman reporters could be adsorbed and distributed in the entire volume of mSiO₂ in a three-dimensional manner, from close to the AuNR surface to the outer surface of the mSiO₂ shell. With the growth of the metal core, the mSiO₂ shell became thinner (from 10 nm

to approximately 8 nm, as shown in Figure S1, Supporting Information). During this process, the Raman reporter is always located at the most sensitive area very close to the surface of the grown NP with the same reporter distribution density. Therefore, the possible difference induced solely from the loss of reporters of the shortened distance comes from the outer mSiO₂ shell far from the metal surface (in the range of 8 to 10 nm), which is a SERS inert portion from the point of view of “single layered reporter” models. Thus, in our three-dimensional Raman reporter distribution model, the SERS intensity was not very sensitive to the mSiO₂ thickness.

To experimentally test this point of view, we synthesized two groups of NP samples, i.e., AuNR@mSiO₂ samples with the same AuNR core but two mSiO₂ shell thicknesses (approximately 10 and 13 nm) and Au@AgNR@mSiO₂ samples with the same Au@AgNR core but two mSiO₂ shell thicknesses (approximately 13 and 16 nm). The SEM images are shown in Figure S11a–d, Supporting Information. Then, the samples were mixed with 10⁻⁶ M CV for SERS detection. As illustrated in Figure S11e,f, Supporting Information, the SERS intensities were nearly the same for the samples with the same metal cores but different mSiO₂ shell thicknesses. This result implies that, in our model, the SERS intensity changes during the overgrowth reaction are not mainly attributed to the thickness variation of mSiO₂ but rather to the changing of the Raman enhancing ability of the metal NPs.

Kneipp et al.¹ proposed that the SERS Stokes signal, $P^{\text{SERS}}(\nu_s)$, can be estimated as

$$P^{\text{SERS}}(\nu_s) = N\sigma_{\text{ads}}^{\text{R}} |A(\nu_L)|^2 |A(\nu_s)|^2 I(\nu_L)$$

where $I(\nu_L)$ is the excitation laser intensity, $\sigma_{\text{ads}}^{\text{R}}$ is the Raman cross section of the adsorbed molecule, N is the number of molecules that undergo the SERS process, and $A(\nu_L)$ and $A(\nu_s)$ are the laser and Raman scattering field enhancement factors, respectively. From this equation, $A(\nu_L)$, $A(\nu_s)$, and N are the

factors that determine the SERS enhancing ability of the substrate. In our experiment, during the *in situ* NP growth process, $A(\nu_L)$ and $A(\nu_S)$ may have changed as a result of the varying optical features of the metal NPs. Additionally, N increased because the increasing size of the NPs resulted in an enlarged surface area of the NP, causing the Raman signal of more reporters to be enhanced. Therefore, our method gave an “overall” SERS enhancing ability comparison result related to all three factors.

Optical Imaging of Living Cells. For biological imaging applications, the cytotoxicity of Au@AgNRs@mSiO₂ NPs was first estimated by MTT assays on MCF-7 breast cancer cells. The results indicated that there were no significant decreases in cell viability after incubation at a dose of 10 $\mu\text{g mL}^{-1}$ (Figure 5a). Furthermore, we investigated the intracellular SERS performance of the NPs by a Raman microscope equipped with a 632.8 nm laser. Figure 5b,c shows the bright and dark field images of the MCF-7 cells after NP incubation, respectively. It can be observed that the Au@AgNRs@mSiO₂ NPs were distributed in cytoplasmic regions rather than in the nucleus, which might be because the NPs were too large to penetrate into the nucleus. As shown in Figure 5c, the SERS spectra from different locations of one cell show strong signals appearing at the cytoplasm, whereas the signal at the nucleus was very weak. Moreover, the Raman fingerprint signal of CV remained robust and no obvious interference signals were observed because of the protection of the mSiO₂ layer.

CONCLUSION

We herein demonstrated dynamic SERS enhancing ability monitoring of growing noble metal nanostructures via a simplified spatially confined growth method. By taking advantage of the elastic property of the mesoporous silica coating, core-shell metallic NPs could be directly synthesized with no need for interior void pregeneration, which simplified the spatially confined growth procedure. Additionally, by adding Raman reporters to the reaction media, the Raman enhancing ability of instantly growing NPs could be dynamically monitored, demonstrating a greatly enhanced SERS feature of core-shell structures compared to AuNR seeds. Moreover, the resultant Raman reporter-labeled NPs could serve as effective SERS tags for living cells.

The SERS enhanced stability comparison of single noble metal NPs with similar structures was an important and difficult task. Our strategy overcame the aggregation of NPs and Raman reporter adsorption differences on NPs, the two main problems in traditional NP-Raman reporter mixing methods, which potentially induce result distortion by several orders of magnitude. Although the enhancing ability comparison results in our work are not “absolutely precise” because of the mSiO₂ shell thickness variation during the metal core NP growth, the influence of this factor is much less significant than the two mentioned above. Therefore, this method is meaningful and may offer useful SERS information on NPs in a facile way. We believe that this method can be more robust by improving the synthesis quality and repeatability of the core NPs^{45,46} and mSiO₂ shell^{47,48} and may be expanded to SERS investigation of more types and shapes of NPs, which will be useful for screening SERS tags with precisely tuned structures and optical properties.

ASSOCIATED CONTENT

Supporting Information

Mesoporous silica shell thickness distribution histograms. EDX characterization of the samples, UV-vis-NIR spectra evolution of Au@AgNR@mSiO₂ NPs upon the addition of H₂O₂. The characterization of samples after a Ag overcoating reaction performed at low temperature (20 °C) and with AuNR@mSiO₂ seeds of a thicker mSiO₂ shell (30 nm). SEM image and UV-vis-NIR spectra of Au@AuNR@mSiO₂ NPs. SERS comparison results of Au@Ag NPs with the simple NP-Raman reporter mixing method. The SEM images illustrating the NP synthesizing reproducibility. The illustrations and discussions on the single layer reporter models and the three-dimensional reporter distribution model. The influence of mSiO₂ shell thickness on SERS intensity. This material is available free of charge via the Internet at <http://pubs.acs.org>.

AUTHOR INFORMATION

Corresponding Authors

*E-mail: yqwang@yic.ac.cn. Fax: +86 535 2109130. Tel: +86 535 2109130.

*E-mail: lxchen@yic.ac.cn. Fax: +86 535 2109130. Tel: +86 535 2109130.

Notes

The authors declare no competing financial interest.

ACKNOWLEDGMENTS

Financial support from the National Natural Science Foundation of China (81102415, 21305157, and 21275158), the Science and Technology Development Plan of Shandong Province of China (2014GGF01074), and the Natural Science Foundation of Shandong of China (ZR2010BQ012) is gratefully acknowledged.

REFERENCES

- (1) Kneipp, K.; Kneipp, H.; Kneipp, J. Surface-Enhanced Raman Scattering in Local Optical Fields of Silver and Gold Nanoaggregates—From Single-Molecule Raman Spectroscopy to Ultrasensitive Probing in Live Cells. *Acc. Chem. Res.* **2006**, *39*, 443–450.
- (2) Abramczyk, H.; Brozek-Pluska, B. Raman Imaging in Biochemical and Biomedical Applications. Diagnosis and Treatment of Breast Cancer. *Chem. Rev.* **2013**, *113*, 5766–5781.
- (3) Wang, Y.; Yan, B.; Chen, L. SERS Tags: Novel Optical Nanoprobes for Bioanalysis. *Chem. Rev.* **2013**, *113*, 1391–1428.
- (4) Lin, D.; Qin, T.; Wang, Y.; Sun, X.; Chen, L. Graphene Oxide Wrapped SERS Tags: Multifunctional Platforms toward Optical Labeling, Photothermal Ablation of Bacteria, and the Monitoring of Killing Effect. *ACS Appl. Mater. Interfaces* **2014**, *6*, 1320–1329.
- (5) Niu, X.; Chen, H.; Wang, Y.; Wang, W.; Sun, X.; Chen, L. Upconversion Fluorescence-SERS Dual-Mode Tags for Cellular and *In Vivo* Imaging. *ACS Appl. Mater. Interfaces* **2014**, *6*, 5152–5160.
- (6) Lee, S.; Chon, H.; Yoon, S. Y.; Lee, E. K.; Chang, S. I.; Lim, D. W.; Choo, J. Fabrication of SERS-Fluorescence Dual Modal Nanoprobes and Application to Multiplex Cancer Cell Imaging. *Nanoscale* **2011**, *4*, 124–129.
- (7) Chung, E.; Gao, R.; Ko, J.; Choi, N.; Lim, D. W.; Lee, E. K.; Chang, S. I.; Choo, J. Trace Analysis of Mercury(II) Ions Using Aptamer-Modified Au/Ag Core-Shell Nanoparticles and SERS Spectroscopy in a Microdroplet Channel. *Lab Chip* **2013**, *13*, 260–266.
- (8) Lim, D. K.; Kim, I. J.; Nam, J. M. DNA-Embedded Au/Ag Core-Shell Nanoparticles. *Chem. Commun.* **2008**, 5312–5314.
- (9) Feng, Y.; Wang, Y.; Wang, H.; Chen, T.; Tay, Y. Y.; Yao, L.; Yan, Q.; Li, S.; Chen, H. Engineering “Hot” Nanoparticles for Surface-Enhanced Raman Scattering by Embedding Reporter Molecules in Metal Layers. *Small* **2011**, *8*, 246–251.

- (10) Zhou, Y.; Lee, C.; Zhang, J.; Zhang, P. Engineering Versatile SERS-Active Nanoparticles by Embedding Reporters between Au-Core/Ag-Shell through Layer-by-Layer Deposited Polyelectrolytes. *J. Mater. Chem. C* **2013**, *1*, 3695–3699.
- (11) Liu, Z.; Yang, Z.; Peng, B.; Cao, C.; Zhang, C.; You, H.; Xiong, Q.; Li, Z.; Fang, J. Highly Sensitive, Uniform, and Reproducible Surface-Enhanced Raman Spectroscopy from Hollow Au-Ag Alloy Nanorattles. *Adv. Mater.* **2014**, *26*, 2431–2439.
- (12) Huang, J.; Kim, K. H.; Choi, N.; Chon, H.; Lee, S.; Choo, J. Preparation of Silica-Encapsulated Hollow Gold Nanosphere Tags Using Layer-by-Layer Method for Multiplex Surface-Enhanced Raman Scattering Detection. *Langmuir* **2011**, *27*, 10228–10233.
- (13) Gandra, N.; Singamaneni, S. Bilayered Raman-Intense Gold Nanostructures with Hidden Tags (BRIGHTS) for High-Resolution Bioimaging. *Adv. Mater.* **2013**, *25*, 1022–1027.
- (14) Gandra, N.; Portz, C.; Singamaneni, S. Multifunctional Plasmonic Nanorattles for Spectrum-Guided Locoregional Therapy. *Adv. Mater.* **2014**, *26*, 424–429.
- (15) Jaiswal, A.; Tian, L.; Tadepalli, S.; Liu, K. K.; Fei, M.; Farrell, M. E.; Pellegrino, P. M.; Singamaneni, S. Plasmonic Nanorattles with Intrinsic Electromagnetic Hot-Spots for Surface Enhanced Raman Scattering. *Small* **2014**, *10*, 4287–4292.
- (16) Darby, B. L.; Le Ru, E. C. Competition between Molecular Adsorption and Diffusion: Dramatic Consequences for SERS in Colloidal Solutions. *J. Am. Chem. Soc.* **2014**, *136*, 10965–10973.
- (17) Chen, G.; Wang, Y.; Yang, M.; Xu, J.; Goh, S. J.; Pan, M.; Chen, H. Measuring Ensemble-Averaged Surface-Enhanced Raman Scattering in the Hotspots of Colloidal Nanoparticle Dimers and Trimers. *J. Am. Chem. Soc.* **2010**, *132*, 3644–3645.
- (18) Braun, G. B.; Lee, S. J.; Laurence, T.; Fera, N.; Fabris, L.; Bazan, G. C.; Moskovits, M.; Reich, N. O. Generalized Approach to SERS-Active Nanomaterials Via Controlled Nanoparticle Linking, Polymer Encapsulation, and Small-Molecule Infusion. *J. Phys. Chem. C* **2009**, *113*, 13622–13629.
- (19) Roca, M.; Haes, A. J. Silica-Void-Gold Nanoparticles: Temporally Stable Surface-Enhanced Raman Scattering Substrates. *J. Am. Chem. Soc.* **2008**, *130*, 14273–14279.
- (20) Zhang, W.; Wang, Y.; Sun, X.; Wang, W.; Chen, L. Mesoporous Titania Based Yolk-Shell Nanoparticles as Multifunctional Theranostic Platforms for SERS Imaging and Chemo-Photothermal Treatment. *Nanoscale* **2014**, *6*, 14514–14522.
- (21) Wang, G. Q.; Chen, Z. P.; Chen, L. X. Mesoporous Silica-Coated Gold Nanorods: Towards Sensitive Colorimetric Sensing of Ascorbic Acid via Target-Induced Silver Overcoating. *Nanoscale* **2011**, *3*, 1756–1759.
- (22) Zhang, Q.; Ge, J.; Goebel, J.; Hu, Y.; Sun, Y.; Yin, Y. Tailored Synthesis of Superparamagnetic Gold Nanoshells with Tunable Optical Properties. *Adv. Mater.* **2010**, *22*, 1905–1909.
- (23) Xiao, M.; Zhao, C.; Chen, H.; Yang, B.; Wang, J. “Ship-in-a-Bottle” Growth of Noble Metal Nanostructures. *Adv. Funct. Mater.* **2012**, *22*, 4526–4532.
- (24) Yang, J.; Shen, D.; Zhou, L.; Li, W.; Li, X.; Yao, C.; Wang, R.; El-Toni, A. M.; Zhang, F.; Zhao, D. Spatially Confined Fabrication of Core-Shell Gold Nanocages@Mesoporous Silica for Near-Infrared Controlled Photothermal Drug Release. *Chem. Mater.* **2013**, *25*, 3030–3037.
- (25) Tan, L. F.; Wu, X. L.; Chen, D.; Liu, H. Y.; Meng, X. W.; Tang, F. Q. Confining Alloy or Core-Shell Au-Pd Bimetallic Nanocrystals in Silica Nanorattles for Enhanced Catalytic Performance. *J. Mater. Chem. A* **2013**, *1*, 10382–10388.
- (26) Angelome, P. C.; Pastoriza-Santos, I.; Perez-Juste, J.; Rodriguez-Gonzalez, B.; Zelcer, A.; Soler-Illia, G. J.; Liz-Marzan, L. M. Growth and Branching of Gold Nanoparticles through Mesoporous Silica Thin Films. *Nanoscale* **2012**, *4*, 931–939.
- (27) Choi, E.; Kwak, M.; Jang, B.; Piao, Y. Highly Monodisperse Rattle-Structured Nanomaterials with Gold Nanorod Core-Mesoporous Silica Shell as Drug Delivery Vehicles and Nanoreactors. *Nanoscale* **2013**, *5*, 151–154.
- (28) Nikoobakht, B.; El-Sayed, M. A. Preparation and Growth Mechanism of Gold Nanorods (NRs) Using Seed-Mediated Growth Method. *Chem. Mater.* **2003**, *15*, 1957–1962.
- (29) Gorelikov, I.; Matsuura, N. Single-Step Coating of Mesoporous Silica on Cetyltrimethyl Ammonium Bromide-Capped Nanoparticles. *Nano Lett.* **2008**, *8*, 369–373.
- (30) Khlebtsov, B. N.; Khanadeev, V. A.; Tsvetkov, M. Y.; Bagratashvili, V. N.; Khlebtsov, N. G. Surface-Enhanced Raman Scattering Substrates Based on Self-Assembled Pegylated Gold and Gold-Silver Core-Shell Nanorods. *J. Phys. Chem. C* **2013**, *117*, 23162–23171.
- (31) Xiang, Y. U.; Wu, X. C.; Liu, D. F.; Li, Z. Y.; Chu, W. G.; Feng, L. L.; Zhang, K.; Zhou, W. Y.; Xie, S. S. Gold Nanorod-Seeded Growth of Silver Nanostructures: From Homogeneous Coating to Anisotropic Coating. *Langmuir* **2008**, *24*, 3465–3470.
- (32) Wang, G. Q.; Chen, Z. P.; Wang, W. H.; Yan, B.; Chen, L. X. Chemical Redox-Regulated Mesoporous Silica-Coated Gold Nanorods for Colorimetric Probing of Hg²⁺ and S²⁻. *Analyst* **2011**, *136*, 174–178.
- (33) Zhang, C.; Yin, A. X.; Jiang, R. B.; Rong, J.; Dong, L.; Zhao, T.; Sun, L. D.; Wang, J. F.; Chen, X.; Yan, C. H. Time-Temperature Indicator for Perishable Products Based on Kinetically Programmable Ag Overgrowth on Au Nanorods. *ACS Nano* **2013**, *7*, 4561–4568.
- (34) Kim, J.; Kim, H. S.; Lee, N.; Kim, T.; Kim, H.; Yu, T.; Song, I. C.; Moon, W. K.; Hyeon, T. Multifunctional Uniform Nanoparticles Composed of a Magnetite Nanocrystal Core and a Mesoporous Silica Shell for Magnetic Resonance and Fluorescence Imaging and for Drug Delivery. *Angew. Chem., Int. Ed.* **2008**, *47*, 8438–8441.
- (35) Kim, M. H.; Na, H. K.; Kim, Y. K.; Ryoo, S. R.; Cho, H. S.; Lee, K. E.; Jeon, H.; Ryoo, R.; Min, D. H. Facile Synthesis of Monodispersed Mesoporous Silica Nanoparticles with Ultralarge Pores and Their Application in Gene Delivery. *ACS Nano* **2011**, *5*, 3568–3576.
- (36) Sivapalan, S. T.; DeVetter, B. M.; Yang, T. K.; van Dijk, T.; Schulmerich, M. V.; Carney, P. S.; Bhargava, R.; Murphy, C. J. Off-Resonance Surface-Enhanced Raman Spectroscopy from Gold Nanorod Suspensions as a Function of Aspect Ratio: Not What We Thought. *ACS Nano* **2013**, *7*, 2099–2105.
- (37) Abalde-Cela, S.; Aldeanueva-Potel, P.; Mateo-Mateo, C.; Rodriguez-Lorenzo, L.; Alvarez-Puebla, R. A.; Liz-Marzan, L. M. Surface-Enhanced Raman Scattering Biomedical Applications of Plasmonic Colloidal Particles. *J. R. Soc., Interface* **2010**, *7*, S435–S450.
- (38) Xiong, W.; Sikdar, D.; Walsh, M.; Si, K. J.; Tang, Y.; Chen, Y.; Mazid, R.; Weyland, M.; Rukhlenko, I. D.; Etheridge, J.; Premaratne, M.; Li, X.; Cheng, W. Single-Crystal Caged Gold Nanorods with Tunable Broadband Plasmon Resonances. *Chem. Commun.* **2013**, *49*, 9630–9632.
- (39) Ye, X.; Shi, H.; He, X.; Wang, K.; Li, D.; Qiu, P. Gold Nanorod-Seeded Synthesis of Au@Ag/Au Nanospheres with Broad and Intense Near-Infrared Absorption for Photothermal Cancer Therapy. *J. Mater. Chem. B* **2014**, *2*, 3667.
- (40) Shi, H.; Ye, X.; He, X.; Wang, K.; Cui, W.; He, D.; Li, D.; Jia, X. Au@Ag/Au Nanoparticles Assembled with Activatable Aptamer Probes as Smart “Nano-Doctors” for Image-Guided Cancer Thermotherapy. *Nanoscale* **2014**, *6*, 8754–8761.
- (41) Lin, C. C.; Chang, C. W. AuNPs@mesoSiO₂ Composites for SERS Detection of DTNB Molecule. *Biosens. Bioelectron.* **2014**, *51*, 297–303.
- (42) Stiles, P. L.; Dieringer, J. A.; Shah, N. C.; Van Duyne, R. P. Surface-Enhanced Raman Spectroscopy. *Annu. Rev. Anal. Chem.* **2008**, *1*, 601–626.
- (43) Li, J. F.; Huang, Y. F.; Ding, Y.; Yang, Z. L.; Li, S. B.; Zhou, X. S.; Fan, F. R.; Zhang, W.; Zhou, Z. Y.; Wu, D. Y.; Ren, B.; Wang, Z. L.; Tian, Z. Q. Shell-Isolated Nanoparticle-Enhanced Raman Spectroscopy. *Nature* **2010**, *464*, 392–395.
- (44) Lim, D. K.; Jeon, K. S.; Kim, H. M.; Nam, J. M.; Suh, Y. D. Nanogap-Engineerable Raman-Active Nanodumbbells for Single-Molecule Detection. *Nat. Mater.* **2010**, *9*, 60–67.

(45) Zhang, L. M.; Xia, K.; Lu, Z. X.; Li, G. P.; Chen, J.; Deng, Y.; Li, S.; Zhou, F. M.; He, N. Y. Efficient and Facile Synthesis of Gold Nanorods with Finely Tunable Plasmonic Peaks from Visible to Near-Ir Range. *Chem. Mater.* **2014**, *26*, 1794–1798.

(46) Zhang, L. M.; Xia, K.; Bai, Y. Y.; Lu, Z. X.; Tang, Y. J.; Deng, Y.; Chen, J.; Qian, W. P.; Shen, H.; Zhang, Z. J.; Ju, S. H.; He, N. Y. Synthesis of Gold Nanorods and Their Functionalization with Bovine Serum Albumin for Optical Hyperthermia. *J. Biomed. Nanotechnol.* **2014**, *10*, 1440–1449.

(47) Feng, J.; Chang, D.; Wang, Z. F.; Shen, B.; Yang, J. J.; Jiang, Y. Y.; Ju, S. H.; He, N. Y. A FITC-Doped Silica Coated Gold Nanocomposite for Both in Vivo X-ray CT and Fluorescence Dual Modal Imaging. *RSC Adv.* **2014**, *4*, 51950–51959.

(48) Feng, J.; Wang, Z. F.; Shen, B.; Zhang, L. M.; Yang, X.; He, N. Y. Effects of Template Removal on Both Morphology of Mesoporous Silica-Coated Gold Nanorod and Its Biomedical Application. *RSC Adv.* **2014**, *4*, 28683–28690.